Influence of Different Spherical Binary Plasmonic NPs on HTM Layer in Methyl Ammonium Lead Triiodide Solar Cell

Cliff Orori Mosiori [1] **, Walter Kamande Njoroge** [1] **, Lawrence Otieno Ochoo** [1]

[1] *Kenyatta University*
P. O. Box 43844-00100, Nairobi, Kenya

Corresponding Author:
Cliff Orori Mosiori
corori@tum.ac.ke

Abstract. Methylammonium lead triiodide perovskite solar cells have attracted huge research interest. Its optoelectronic properties are competing with those of silicon wafers. It is a hybrid absorber with a direct band gap of about 1.53 eV with good light-absorption capability appropriate for optoelectronic applications. A typical perovskite solar cell HTML layer rarely incorporates ZnO or Cu_2O or TiO_2 nanoparticles to increase charge carrier transport. These ZnO, Cu_2O, TiO_2 nanoparticles can be introduced into the HTM layer to modify its PSCs efficiency and performance. These nanoparticles are direct band gap binary semiconductors with a wide band gap energy range of 2.17 eV to 3.37 eV respectively which can lead to higher transport mobility and enhanced HTM nanostructured layer. In this paper, two model solar cell having a $ITO/TiO_2/CH_3NH_3PbI_3/P3HT/Ag$ and $ITO/TiO_2/Ag:CH_3NH_3PbI_3/P3HT/Ag$ structures were proposed, geometrically modelled and simulated using SCAPS-1D software. Their HTM layer (composed of P3HT) was doped with ZnO, Cu_2O, and TiO_2 nanoparticles respectively to determine their influence on PCEs of this solar cells. It was revealed that starting from undoped P3HT layer all through the Cu_2O, ZnO to TIO_2 doped layers, efficiency reduced from 13.123 % and 9.071% respectively; fill factor (FF) also reduced from 69.4% to 48.9 % for the doped CH3NH3PbI3 perovskite solar cell while efficiency of doped $CH_3NH_3PbI_3$ perovskite solar cell reduced from 13.033 % and 9.091%, the fill factor (FF) also reduced from 66.4% to 52.9 % respectively. It was noted that the solar cell employing P3HT undoped layer had the best performance and concluded that introducing nanoparticles onto P3HT layer has a negative impact on the performance of CH3NH3PbI3 perovskite solar cell.

Keywords: Plasmonic Oscillations; hybrid perovskite; SCAPS-1D software; photon absorption; Computer Simulation Technology.

INTRODUCTION

Modern thin-film solar cells have reduced material consumption [2] and fabrication costs. However, a major limitation facing hybrid perovskite thin-film solar cells is its poor photon absorption [1]. It is documented that light-trapping can be increased by increasing the optical path length inside a film, but how to implement it remains a mirage [4]. Plasmonic structures can modify the excitations of localized surface plasmon to improve photon absorption [5]. Surface plasmon is a collective oscillation of free exciting electrons of metallic nanoparticles [5, 7, 9] which can be used to enhance optical absorption through scattering and near-field concentration photons depending on particle shape [11], size [15], inter-particle distance [22], optical resonance [25], material nature [34] and type of coupled systems available [29]. However, plasmon coupling only occurs when closely spaced nanoparticles have their associated electron oscillations influencing its local field affect electron oscillations of neighbouring particles [28, 31, 33]. Many noble metallic nanoparticles have been tested for plasmonic coupling. These include gold (Au), copper (Cu), silver (Ag) and aluminium (Al) nanoparticles [9, 12, 18]. Their dipole and quadrupole plasmon resonances can be described qualitatively using spherical nanoparticles [20, 26]. They have already shown a red-shift in total absorption flux enhancement and tunable localized surface plasmon resonance. The role of near-field coupling, resonance, scattering and transmission of light have been investigated too using Ag nanoparticles [6, 11, 27]. An enhancement factor of 2.3 in external quantum efficiency

at 1100 nm wavelength, a sevenfold enhancement of light absorption and a 16-fold enhancement for 1250 nm using Ag nanoparticles have been reported by some publications [14, 18, 25, 33]. This paper focuses on the doping the HTM layer and its influence on the efficiency of methylammonium lead triiodide solar cells as simulated using SCAPS-1D software at AM1.5G solar radiation that employs FDTD, FEM, and FIT methods.

SCAPS-1D simulation software. SCAPS-1D is a one-dimensional solar cell simulation software that employs three coupled differential equations. The first equation is the Poisson's equation given as (1):

$$\frac{\partial}{\partial x}\left((-\varepsilon_{(x)})\frac{d\varphi}{dx}\right) =$$
$$= q\left[\begin{array}{c}p_{(x)} - n_{(x)} - N_{d(x)}^+ - N_{a(x)}^- + \\ + p_{t(x)} - n_{t(x)}\end{array}\right], \qquad (1)$$

where ψ is electrostatic potential, q is electron charge, p is free holes, n is free electrons, p_t is trapped holes, n_t is trapped electrons, N_a^- is ionized acceptor-like doping concentration, and N_d^+ is ionized donor-like doping concentration [24, 30].

The second equation (2) is the continuity equation for holes as [2, 5, 11]:

$$\frac{dp_n}{dt} = G_p - \frac{p_n - p_{no}}{\tau_p} - p_n\mu_p\frac{d\xi}{dx} -$$
$$- \mu_p\xi\frac{dp_n}{dx} + D_p\frac{\partial^2 p_n}{\partial x^2} \qquad (2)$$

while the 3 equations is the continuity equation for electrons as:

$$\frac{dn_p}{dt} = G_n - \frac{n_p - n_{po}}{\tau_n} - n_p\mu_n\frac{d\xi}{dx} -$$
$$- \mu_n\xi\frac{dn_p}{dx} + D_n\frac{\partial^2 n_p}{\partial x^2} \qquad (3)$$

where G is generation rate, ξ is permittivity while D is the diffusion coefficient.

Computer Simulation Technology. Computer Simulation Technology (CST) is a 3D simulation software used to numerically calculate optical properties required for many applications that include plasmonic solar cells, electromagnet metamaterials and antennas when exposed to an electromagnetic field. It is a 3D EM solver that solves Maxwell's equation in the time domain with Finite integration method (FIT) and frequency domain with the Finite element method (FEM) by incorporating FDTD and FDFD techniques. CST software is a Multiphysics software that employs FIT, FEM, FDTD and FDFD to simulate designed plasmonic nanostructures of various PV devices. CST is a 3D simulation software used in order to attain accurate simulation results under the absorption profile and internal quantum efficiency as a function spatial position, photon density and frequency. It employs FDTD technique to evaluate electron transport, series resistance and fill factor enhancement, distribution profile of the photons absorbed and also electron-hole pair recombination rate. It is a time domain technique used to solve Maxwell's equations in differential form over a grid-based domain in a single simulation by calculating electric field, E, and magnetic field, B for time irrespective of the designed 1D, 2D and 3D models expressed as [14, 15, 23]:

$$\frac{\partial}{\partial t}B(\hat{R},t) = -\nabla \times E(\hat{R},t) - J_m(\hat{R},t) \qquad (4)$$
$$\frac{\partial}{\partial t}D(\hat{R},t) = \nabla \times H(\hat{R},t) - J_e(\hat{R},t) \qquad (4)$$

It reveals nano-structural shapes, material types, dielectric environments, array pitches and particle locations for the source of light scattering. Its optical computational power provides the final power conversion efficiency of plasmonic solar cells. FEM available in CST software and it is used to calculate solutions to partial differential and integral Maxwell's equations. It is suitable for simulating irregular shaped geometrical models for optical devices as it provides information even of large dtime and frequency domains small elements in regions where fields may abruptly change. It can also simulate larger elements in less important and unexpected electromagnet regions.

METHODOLOGY

Device Structures. A plasmonic model solar cell was designed containing silver nanoparticle doped and undoped methylammonium lead triiodide ($CH_3NH_3PbI_3$) as a perovskite absorber layer. The solar cell had five layers as a glass cover (*protection purposes*), an anode (*transparent conducting film*), substrate (*glass*), *n*-type compact layer, absorber layer (*Ag:CH₃NH₃PbI₃ and/or CH₃NH₃PbI₃*), P3HT (*p-type hole transport layer*) and a cathode (*silver*) designed according to [35] as shown in Figure 1.
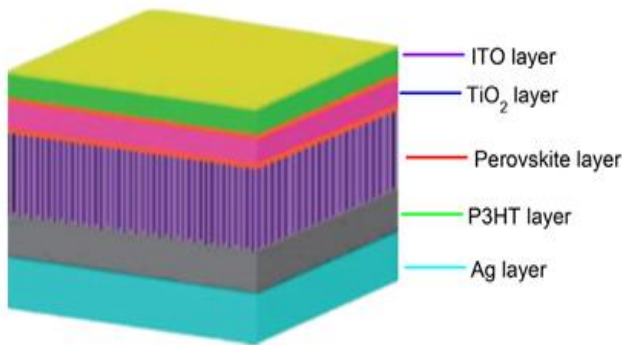
Figure 1 − CH$_3$NH$_3$PbI$_3$ device structure

It was modeled as shown in Figure 2. All the models were considered to be solid-state planar heterojunction *p-i-n* solar cells with low p-type-doped $CH_3NH_3PbI_3$ sandwiched between the *n*-type ETM (compact TiO_2) and *p*-type HTM (P3HT) layers according to [15].

Simulations were performed using light that propagated along *z* direction, through TiO_2, $CH_3NH_3PbI_3$ and entering P3HT hole transporting layer in that order.

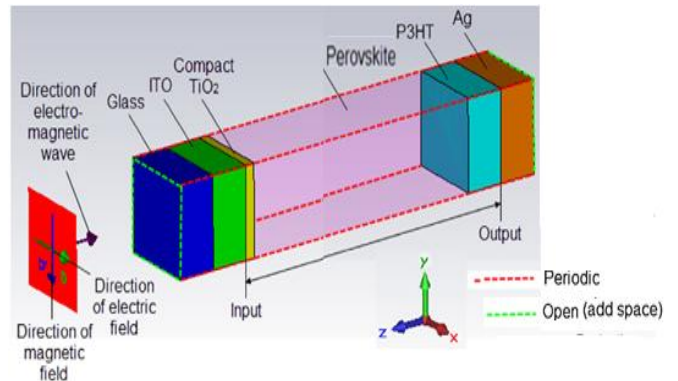Figure 2 − CH$_3$NH$_3$PbI$_3$ device structure

The same design was maintained for the one with or without the silver nanoparticle in its perovskite layer. The *p*-type hole transport (P3HT) layer also modelled as doped with ZnO, Cu_2O and TiO_2 nanoparticles separately and simulated using CST (microwave studio). Numerical simulation using SCAPS-1D simulation software was carried out to analysed the electrical parameters and the PCEs of the resulting solar cells. Table 1 and Table 2 shows the model parameter of the solar cells that were simulated.

Table 1 − Layer arrangement in CH$_3$NH$_3$PbI$_3$ device structure

No	Dopant NPs	Dopant on (HTM)	Device layer structure
A1		P3HT	*ITO/TiO₂/CH₃NH₃PbI₃/P3HT/Ag*
A2	ZnO	P3HT:ZnO	*ITO/TiO₂/CH₃NH₃PbI₃/P3HT:ZnO/Ag*
A3	Cu₂O	P3HT:Cu₂O	*ITO/TiO₂/CH₃NH₃PbI₃/P3HT:Cu₂O/Ag*
A4	TiO₂	P3HT:TiO₂	*ITO/TiO₂/CH₃NH₃PbI₃/P3HT:TiO₂/Ag*

Table 2 − Layer arrangement in CH$_3$NH$_3$PbI$_3$ device structure

No	Dopant NPs	Dopant on (HTM)	Device layer structure
B1	-	P3HT	*ITO/TiO₂/Ag:CH₃NH₃PbI₃/P3HT/Ag*
B2	ZnO	P3HT:ZnO	*ITO/TiO₂/Ag:CH₃NH₃PbI₃/P3HT:ZnO/Ag*
B3	Cu₂O	P3HT:Cu₂O	*ITO/TiO₂/Ag:CH₃NH₃PbI₃/P3HT:Cu₂O/Ag*
B4	TiO₂	P3HT:TiO₂	*ITO/TiO₂/Ag:CH₃NH₃PbI₃/P3HT:TiO₂/Ag*

Device Simulation. Two simulation software were used in this work. The SCAPS-1D simulation software was used to numerically simulate photovoltaic cell analysis while other parameters were simulated using Computer Simulation Technology (CST) software. These are easy to use software's available from authorized vendors.

The solar cell models in Table 1 and Table 2 were simulated.

Choice of simulation parameters. The material optical parameters used in SCAPS-1D simulation were selectively picked from published articles by [35] and a number of supporting optoelectronic theories. The other optical constant and absorption coefficients for both $CH_3NH_3PbI_3$ and $Ag:CH_3NH_3PbI_3$ were obtained from [16]. A summary of some of these optical parameters are as tabulated in tables 1. It was adopted that the defect density of 1×10^{10} cm^{-3}, electron hole and thermal velocity of 1.0×10^7 cm/s, donor density, (N_D) of zero (0), defect reference energy level was taken above E_v while energy level reference to 0.7e V respectively. Finally, energetic distribution and reference point for defect energy level (E_t) were assumed to be single and above the highest E_v respectively when simulating the active layers $(CH_3NH_3PbI_3, Ag:CH_3NH_3PbI_3)$ and perovskite/P3HT interface layers. Numerical simulation was finally performed.

Table 3 − Parameters for SCAPS-1D simulation

Parameters	Unit	Ag:CH₃NH₃PbI₃	CH₃NH₃PbI₃
Bandgap	eV	1.662	1.711
Thickness	nm	420	420
Dielectric constant		4.446	10
Electron affinity	eV	4.20	4.11
Density of States (CB)	1/cm³	1.0×10^{18}	2.25×10^{18}
Density of States (VB)	1/cm³	1.0×10^{18}	1.0×10^{18}
Electron mobility	cm²/Vs	1.6	2.20
Hole mobility	cm²/Vs	1.6	2.20
Acceptor density, (N_A)	1/cm³	3.2×10^{15}	1.0×10^{18}
Electron cross-section	cm²	1.0×10^{-16}	1.0×10^{-13}
Hole cross section area	cm²	1.0×10^{-14}	1.0×10^{-13}
Uniform total (Nt)	1/cm³	4.5×10^{16}	1.0×10^{12}

Limitation on Simulations. All simulations were limited to either thickness, defect at hole transporting (HTM) layer, the density of states (DOS) and different nanoparticles on P3HT host HTM layer. As a result, thermal velocity of electrons and holes were taken as equal at 1×10^7 cm/s while an illumination of 1000W/m², temperature of 25°C, and an air mass of 1.5G were adopted and the simulation software was limited to by SCAPS-1D simulation software to determine to short-circuit current density, J_{sc}, open-circuit voltage, V_{oc}, fill factor, FF, and power conversion efficiency, η, for different doped HTM layer. All other simulations were subjected to CST (microwave studio) software.

RESULTS AND DISCUSSIONS

Influence of $CH_3NH_3PbI_3$ and $Ag:CH_3NH_3PbI_3$ layer thickness. Figure 3 shows the variation of thickness of $CH_3NH_3PbI_3$ and $Ag:CH_3NH_3PbI_3$ absorber layers with respect to open-circuit voltage.
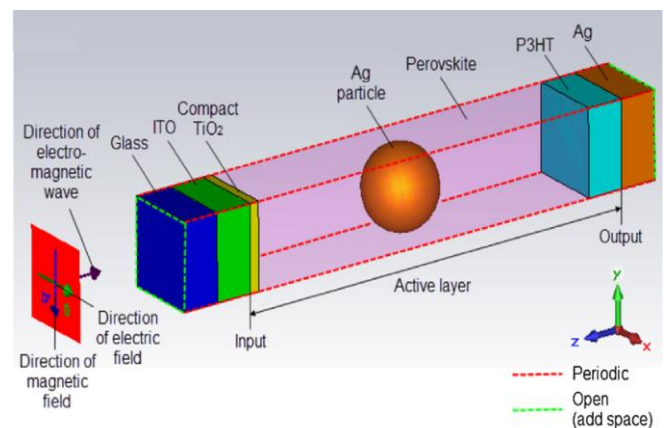
Figure 3 − Ag:CH₃NH₃PbI₃ perovskite solar cell model

It can be noted that the open-circuit voltage of $CH_3NH_3PbI_3$ layer increases gradually as thickness increases to a certain peak point. This in effect implies that the efficiency increases up to a certain value which can be considered as the optimum at a specific thickness. Therefore, with increasing thickness, the short circuit current (J_{sc}) increases and therefore a thicker absorber layer will absorb more photons which in turn, will relatively create more electron-hole pairs resulting in higher open-circuit voltage values. From figure 3 also, it can be observed that a thickness of 320–440 nm is appropriate for Ag:CH₃NH₃PbI₃ perovskite layer for optimal photon absorption based on the AM 1.5G simulation radiation. The optimum thickness that recorded the highest V_{OC} for both Ag:CH₃NH₃PbI₃ and CH₃NH₃PbI₃ layers was 420 nm. The gradual increase in V_{OC} from 280–420 nm was attributed to the plasmonic contributions due to silver nanoparticles with a maximum localized surface plasmonic effect attained at 420 nm. Beyond this thickness, chances of recombination of electron-holes increase as

the charge carriers traverse the longer distance in thick films and therefore diffusion is hampered. Thickness is a major parameter that plays a vital role in the overall performance of the solar cell. It could be the thickness for the absorber layer, HTM layer or the back contact. However, the efficiency of a perovskite solar cell depends largely on its response to the solar spectrum as influenced by thickness.
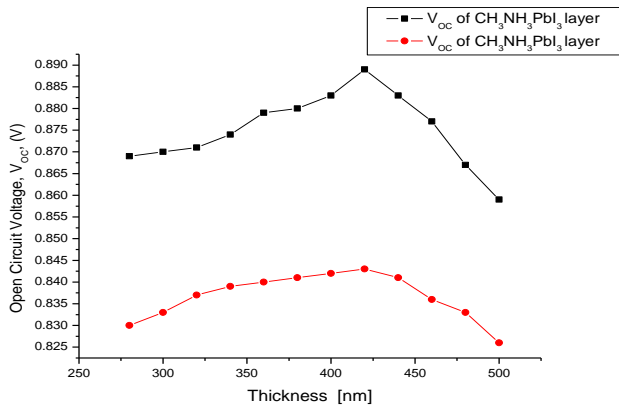

Figure 4 – Influence of thickness on open-circuit voltage perovskite layer

The thickness of $Ag:CH_3NH_3PbI_3$ absorber layer was varied from 280 nm to 500 nm while that of the HTM layer was varied between 28 nm to 50 nm. The simulated V_{OC} was tabulated as shown in figure 1 using table 3. Thin photovoltaic absorber layers are held responsible for less electron-hole recombination. In such cases, dark saturation current remains very low. This means that open-circuit voltage will remain relatively high. In cases where the thickness is increased, the dark saturation current also increases and as a result, open-circuit voltage decreases and in turn efficiency decreases. Normally, for ideal solar cells, the open-circuit voltage is obtained from (5):

$$V_{OC} = \left(\frac{AkT}{q}\right) ln \left(\frac{I_L}{I_O} + 1\right), \qquad (5)$$

where I_0 and I_L are dark saturation current and light-generated current, while kT/q and A are the thermal voltage and the photodiode ideality factor [31].

It also implies that the fill factor of this solar cell will decrease as thickness increase and the consequence will be that the cell internally consumes power reducing efficiency after a certain peak thickness. Similar observations were re-

ported by the experimental result by [16], who concluded that recombination expedites with increasing thickness.

Influence of Defect State at HTM / perovskite Interface Layer. Methyl ammonium lead triiodide films have a number of defects. These include point defects. A defect layer on the $Ag:CH_3NH_3PbI_3/$ HTM interface layer was considered during simulations which took into account the interface recombinations. The simulation parameters used are shown in Table 4.

Table 4 – Parameters simulating perovskite / HTM layer interface layer

Interface layer	Unit	Value/quantity
Capture cross section electrons	cm^2	1.0×10^{-18}
Capture cross section holes	cm^2	1.0×10^{-16}
Energy with respect to reference	eV	0.050
Integrated total density	$1/cm^2$	$1.0 \times 10^{+12}$

Figure 5 shows the effect of interface defect density versus efficiency curves for three different nanoparticle dopants on the HTM layer. From figure 5, it can be noted that there was a negligible effect on efficiency above defect density of 1.12×10^{12} cm^{-3}. When defect density went below 1.01×10^{12} cm^{-3}, a notable decrease in PCEs was recorded.
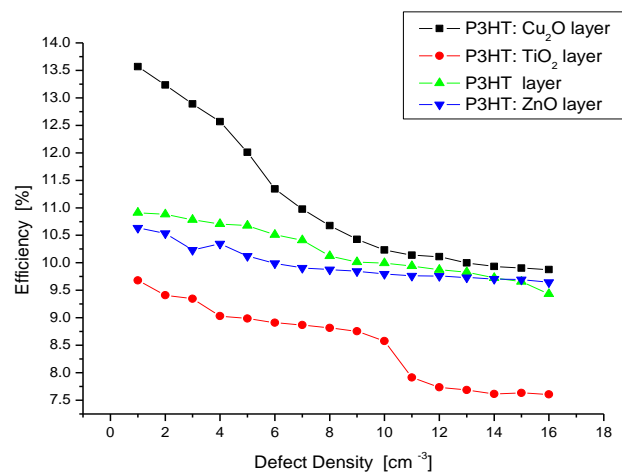

Figure 5 – Defect density of $Ag:CH_3NH_3PbI_3/HTM$ interface layer versus efficiency

With an increase in defect density, the recombination rate increases and as a result efficiency decreases. It was noted that doping P3HT layers with binary impurities reduced its potential as a

HTM layers for hybrid perovskite solar cells. Such attempts have not been carried out through attempts to practically implemented this are on progress. HTM layer can be deposited by sputtering [10], copper oxidation [12, 15], spin coating, atomic layer deposition and even more expensive techniques like molecular beam epitaxial technique.

Influence of Density of State of perovskite Layer. Figure 6 shows the variation of density of state (DOS) with thickness.
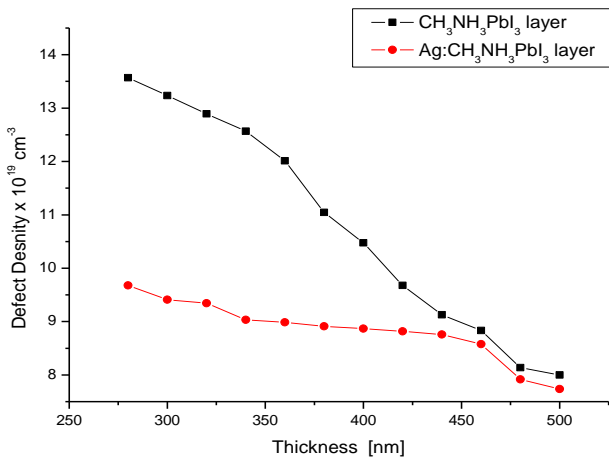

Figure 6 − Defect density of the perovskite layer versus thickness

The effect of DOS of the $CH_3NH_3PbI_3$ perovskite absorber layer was simulated with respect to thickness without accounting on the influence of the doped HTM layers. It can be observed from figure 6 that the density of state (N_v) varied from 13.76×10^{19} cm^{-3} to 7.5×10^{19} cm^{-3} for $CH_3NH_3PbI_3$ layer and from 9.75×10^{19} cm^{-3} to 7.79×10^{19} cm^{-3} for $Ag:CH_3NH_3PbI_3$ layer. This suggested that as thickness increases, the rate of recombination increases and this introduces multiple parasitic capacitances that negative affect solar cell efficiency.

Influence of Valance band effective density of state on efficiency. Figure 7, 8 show the curves of valance band effective density of state versus efficiency for $CH_3NH_3PbI_3$ and $Ag:CH_3NH_3PbI_3$ layers. From the curves in figure 6, it can be noted that in general, the cell efficiency of $CH_3NH_3PbI_3$ absorber layer decreases with the increase in valence band effective density (N_v). As the number of holes increases in the $CH_3NH_3PbI_3$ absorber layer. Their possibility of taking part in reverse saturation current once the solar cell circuit is completed also increases. Consequently, the open-circuit

voltage declines which leads to low electric conversion efficiency and hence poor solar cell performance.

Since low electron affinity of the HTM layer usually has a great significance on charge carrier mobility low affinity safeguards high-hole mobility. As a consequence, carrier mobility in P3HT as a hole transporting layer increases it as a reliable hole transport material (HTM) for hybrid perovskite heterojunction devices.
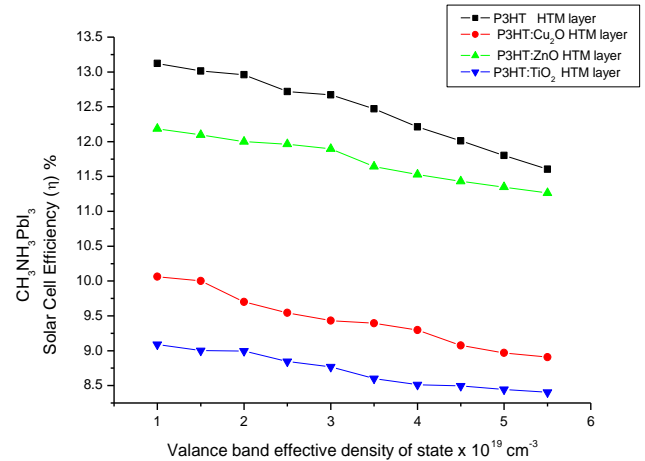

Figure 7 − Valance band effective density of state in $CH_3NH_3PbI_3$ versus cell efficiency
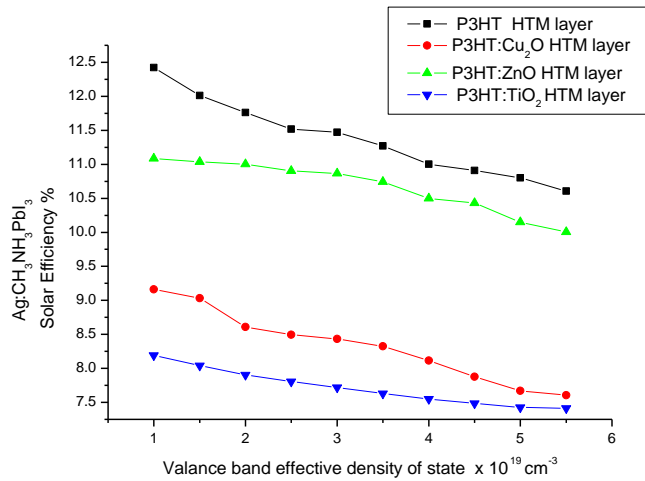

Figure 8 − Valance band effective density of state in $Ag:CH_3NH_3PbI_3$ versus cell efficiency

Influence of silver Back Contacts. Simulations were carried out using the silver metal paste as a prospective back contact for methyl ammonium lead triiodide perovskite solar cells to determine the effect of doping P3HT as its hole transport layer. Parameters used in simulating the back contact are as shown in Table 5 while Table 4 illustrates the simulation result of efficiency. It was ob-

served that the performance of the solar cells decreased depending on the type of nanoparticle material used. Cu_2O dopant had the highest efficiency while TiO_2 dopant had the least efficiency. This showed that doped P3HT was energetically unfavourable for holes to travel towards the silver electrode with an opposing electric field within or close to HTM since the back contact becomes negative.

Table 5 – Parameters for simulating silver back contact

Parameters	Unit	Value/quantity
Surface recombination velocity of electrons	cm/s	$1.0 \times 10^{+5}$
Surface recombination velocity of holes	cm/s	$1.0 \times 10^{+7}$
Metal work function	eV	4.736
Majority carrier barrier height relative to E_f	eV	0.40
Majority carrier barrier height relative to E_v	eV	0.3251

The decrease in efficiency was also attributed to the back contact as shown in Table 6.

Table 6 – Influence of (Ag) back contact

HTM Layer	Thickness (nm)	PCE (%)	% PCE Decrease
P3HT	40	13.123	-
P3HT:ZnO	40	10.062	3.061
P3HT:Cu_2O	40	12.184	2.939
P3HT:TiO_2	40	9.091	4.032

When compared to Au contact used elsewhere [17, 18, 21, 28], it was anticipated that the lower work function of silver metal contact was attributed to the lower efficiency. It was recommended that Au should be given a priority when developing hybrid perovskite solar cells.

Numerical Analysis open-circuit voltage. Figure 4 shows a plot of the variation of open-circuit voltage curves for ZnO, Cu_2O, and TiO_2 nanoparticle dopants against P3HT HTM layer varied between 28–50 nm. For purposes of simulation, the thickness of HTM layer was varied between 28–50 nm at intervals of 2 nm. This thickness is the common thickness is used in many solar cells. The HTM layer containing ZnO, Cu_2O, and TiO_2 nanoparticle dopants in HTM layer were simulated to obtain open voltage currents. Their open-circuit voltages (V_{OC}) were determined as well as their efficiencies. During a simulation,

theoretical constants used to estimate open-circuit voltages (V_{OC}) included the fundamental parameters like bandgap, electron affinity, dielectric permittivity, electron, and hole mobility and how they can influence the HTM layers. The optimum open-circuit voltage obtained was as shown in Figure 4.
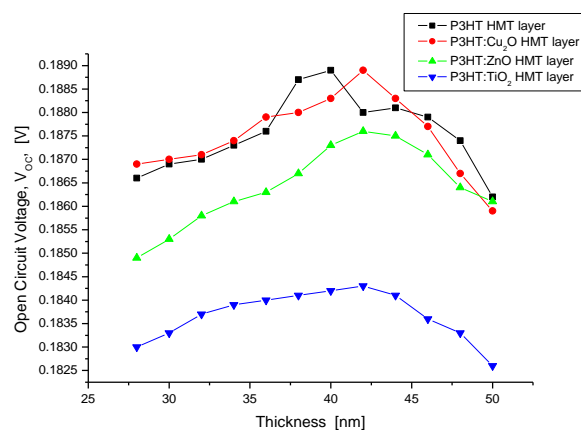

Figure 9 – Influence of HTM thickness on open-circuit voltage

It was observed from Figure 9 that Cu_2O had a very small significant contribution to the open-circuit voltage on P3HT layer as V_{OC} values were relatively close to those of P3HT layer. This suggested that in the presence of P3HT layer, there is no need of introducing Cu_2O nanoparticles. Its plasmonic contributions can be neglected. The presence of ZnO nanoparticles relatively reduced the contribution of P3HT layer to open-circuit voltages of the perovskite layer. The reduction was attributed to the higher recombination within the HTM layer as a result of plasmonic effects due to ZnO nanoparticles. Similarly, TiO_2 registered the highest relative reduction of V_{OC} as compared to all nanoparticles used. This suggested that its plasmonic contribution acted negatively in P3HT hole transport layer and should be neglected at all costs when developing a perovskite solar cell. These observations were attributed to the unique plasmonic properties of the plasmonic particles used.

Model Ag:$CH_3NH_3PbI_3$ perovskite solar cell. For modelling and performing simulation using the SCAPS-1D simulator, structure by doping $CH_3NH_3PbI_3$ using silver nanoparticles and also by doping the P3HT hole transport material interfaced with a silver (Ag) metal back contact. Parameters for simulation were adopted from literature, experimental work and simulation using CST (microwave studio) software.

Table 7 – PC Efficiency of $CH_3NH_3PbI_3$ perovskite solar cell

HTM Layer	V_{OC} (V)	Fill Factor	PCE (%)
P3HT	0.889	69.4	13.123
P3HT:ZnO	0.881	57.6	10.062
P3HT:Cu₂O	0.885	65.3	12.184
P3HT:TiO₂	0.837	52.9	9.091
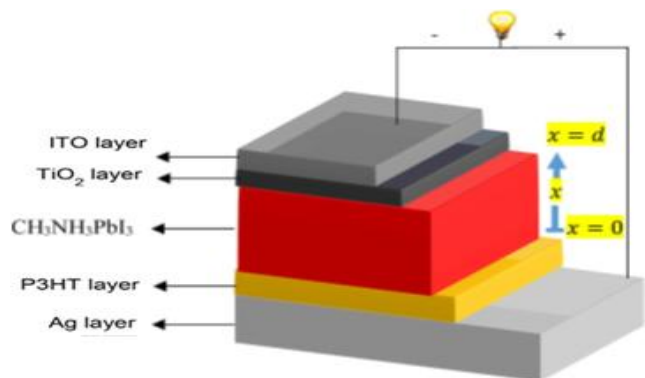
Figure 10 – Model device structure of Ag:$CH_3NH_3PbI_3$ perovskite solar cell

Table 8 – PC Efficiency of Ag:$CH_3NH_3PbI_3$ perovskite solar cell

HTM Layer	V_{OC} (V)	Fill Factor	PCE (%)
P3HT	0.843	66.4	13.033
P3HT:ZnO	0.841	53.6	10.002
P3HT:Cu₂O	0.842	60.3	12.114
P3HT:TiO₂	0.836	48.9	9.071

The HTM layer structure suggested here is different from that proposed by other researches where Ag:$CH_3NH_3PbI_3$ absorber perovskite layer instead of $CH_3NH_3PbI_3$ absorber layer. In all model structures, Cu_2O, ZnO, and TIO_2 were considered as dopant in HTM layer. It was concluded that Cu_2O ensures the highest performance among dopant nanoparticles slightly lower than P3HT layer. This was attributed to the properties of Cu_2O since it is a 2.17 eV direct bandgap *p*-type binary inorganic absorber solar cell material

[23]. Starting from P3HT layer through Cu_2O, ZnO to TiO_2 doped layers, the efficiency of 13.123 % and 9.071% FF range of 69.4% to 48.9 % for $CH_3NH_3PbI_3$ perovskite solar cell and 13.033 % and 9.091% FF range of 66.4% to 52.9 % $CH_3NH_3PbI_3$ perovskite solar cell.

CONCLUSION

As compared to other simulated perovskite solar cell efficiencies, the I-V characteristics obtained in this work reflect the performance outcome expected by this perovskite layer of 450 nm thickness exhibited by a valance band density of states of 3.2×10^{18} cm^{-3} and interface defect density of 1.12×10^{12} cm^{-3} respectively. ITO/ TiO_2/ $CH_3NH_3PbI_3$/P3HT/Ag perovskite structure gave the best performance among all the PSCs simulated. From the findings of this study, it was revealed that among all the simulated solar cells, the solar cell employing P3HT undoped HTM layer had the best performance. Open-circuit voltage and short circuit current changes were significant. This finding shows that we can modify the performance of a hybrid solar cell by modifying its organic HTM layer using binary inorganic plasmonic nanoparticles. It was therefore concluded that these findings can be used to justify the model in this paper as a potential alternative way to developing conventional hybrid perovskite solar cells. It was recommended that experimental investigation was required to determine its viability. It was concluded that binary inorganic nanoparticles hamper the performance of P3HT HTM layer for solar cell applications.

ACKNOWLEDGEMENT

REFERENCES

1. Atwater, H., & Polman, A. (2010). Plasmonics for improved photovoltaic devices. *Nature Materials, 9*, 205–213.

2. Barnes, W. L., Dereux, A., & Ebbesen, T. W. (2003). Surface plasmon subwavelength optics. *Nature, 424*(6950), 824–830. doi: 10.1038/nature01937

3. Beck, F. J., Polman, A., & Catchpole, K. R. (2009). Tunable light trapping for solar cells using localized surface plasmons. *Journal of Applied Physics, 105*(11), 114310. doi: 10.1063/1.3140609

4. Cao, J., Sun, T., & Grattan, K. T. V. (2014). Gold nanorod-based localized surface plasmon resonance biosensors: A review. *Sensors and Actuators B: Chemical, 195*, 332–351. doi: 10.1016/j.snb.2014.01.056

5. Catchpole, K. R., & Polman, A. (2008). Plasmonic solar cells. *Optics Express, 16*(26), 21793. doi: 10.1364/oe.16.021793

6. Derkacs, D., Lim, S. H., Matheu, P., Mar, W., & Yu, E. T. (2006). Improved performance of amorphous silicon solar cells via scattering from surface plasmon polaritons in nearby metallic nanoparticles. *Applied Physics Letters, 89*(9), 093103. doi: 10.1063/1.2336629

7. Duche, D., Torchio, P., Escoubas, L., Monestier, F., Simon, J.-J., Flory, F., & Mathian, G. (2009). Improving light absorption in organic solar cells by plasmonic contribution. *Solar Energy Materials and Solar Cells, 93*(8), 1377–1382. doi: 10.1016/j.solmat.2009.02.028

8. Ghosh, B., Espinoza, G. (2017). Plasmonics for Improved Photovoltaic Devices. *Juniper Online Material Science, 1*(2): 555–558. doi: 10.19080/JOJMS.2017.01.555558

9. Hu, M., Chen, J., Li, Z.-Y., Au, L., Hartland, G. V., Li, X., … Xia, Y. (2006). Gold nanostructures: engineering their plasmonic properties for biomedical applications. *Chemical Society Reviews, 35*(11), 1084. doi: 10.1039/b517615h

10. Kelly, K. L., Coronado, E., Zhao, L. L., & Schatz, G. C. (2003). The Optical Properties of Metal Nanoparticles: The Influence of Size, Shape, and Dielectric Environment. *The Journal of Physical Chemistry B, 107*(3), 668–677. doi: 10.1021/jp026731y

11. Kumar, S., Wittenberg, N. J., & Oh, S.-H. (2012). Nanopore-Induced Spontaneous Concentration for Optofluidic Sensing and Particle Assembly. *Analytical Chemistry, 85*(2), 971–977. doi: 10.1021/ac302690w

12. Lamprecht, B., Schider, G., Lechner, R. T., Ditlbacher, H., Krenn, J. R., Leitner, A., & Aussenegg, F. R. (2000). Metal Nanoparticle Gratings: Influence of Dipolar Particle Interaction on the Plasmon Resonance. *Physical Review Letters, 84*(20), 4721–4724. doi: 10.1103/physrevlett.84.4721

13. Maier, S. A., Brongersma, M. L., Kik, P. G., Meltzer, S., Requicha, A. A. G., Koel, B. E., & Atwater, H. A. (2003). Plasmonics—A Route to Nanoscale Optical Devices (Advanced Materials, 2001, 13, 1501). *Advanced Materials, 15*(78), 562–562. doi: 10.1002/adma.200390134

14. Mansoor, R., & AL-Khursan, A. H. (2018). Numerical modelling of surface plasmonic polaritons. *Results in Physics, 9*, 1297–1300. doi: 10.1016/j.rinp.2018.04.052

15. Moreno, F., García-Cámara, B., Saiz, J. M., & González, F. (2008). Interaction of nanoparticles with substrates: effects on the dipolar behaviour of the particles. *Optics Express, 16*(17), 12487. doi: 10.1364/oe.16.012487

16. Mosiori, C. O., Oeba, D. A., & Shikambe, R. (2017). Determination of Planck's Constant using Light Emitting Diodes. *Path of Science, 3*(10), 2007–2012. doi: 10.22178/pos.27-2

17. Murray, W. A., & Barnes, W. L. (2007). Plasmonic Materials. *Advanced Materials, 19*(22), 3771–3782. doi: 10.1002/adma.200700678

18. Oskooi, A. F., Roundy, D., Ibanescu, M., Bermel, P., Joannopoulos, J. D., & Johnson, S. G. (2010). Meep: A flexible free-software package for electromagnetic simulations by the FDTD method. *Computer Physics Communications, 181*(3), 687–702. doi: 10.1016/j.cpc.2009.11.008

19. Pattnaik, P. (2005). Surface plasmon resonance. *Applied biochemistry and biotechnology, 126*(2), 79–92.

20. Petryayeva, E., & Krull, U. J. (2011). Localized surface plasmon resonance: Nanostructures, bioassays and biosensing – A review. *Analytica Chimica Acta, 706*(1), 8–24. doi: 10.1016/j.aca.2011.08.020

21. Pillai, S., & Green, M. A. (2010). Plasmonics for photovoltaic applications. *Solar Energy Materials and Solar Cells, 94*(9), 1481–1486. doi: 10.1016/j.solmat.2010.02.046

22. Pillai, S., Catchpole, K. R., Trupke, T., & Green, M. A. (2007). Surface plasmon enhanced silicon solar cells. *Journal of Applied Physics, 101*(9), 093105. doi: 10.1063/1.2734885

23. Pirozhenko, I., & Lambrecht, A. (2008). Influence of slab thickness on the Casimir force. *Physical Review A, 77*(1). doi: 10.1103/physreva.77.013811

24. Rechberger, W., Hohenau, A., Leitner, A., Krenn, J. R., Lamprecht, B., & Aussenegg, F. R. (2003). Optical properties of two interacting gold nanoparticles. *Optics Communications, 220*(1-3), 137–141. doi: 10.1016/s0030-4018(03)01357-9

25. Rockstuhl, C., Fahr, S., & Lederer, F. (2008). Absorption enhancement in solar cells by localized plasmon polaritons. *Journal of Applied Physics, 104*(12), 123102. doi: 10.1063/1.3037239

26. Schaadt, D. M., Feng, B., & Yu, E. T. (2005). Enhanced semiconductor optical absorption via surface plasmon excitation in metal nanoparticles. *Applied Physics Letters, 86*(6), 063106. doi: 10.1063/1.1855423

27. Spinelli, P., van Lare, C., Verhagen, E., & Polman, A. (2011). Controlling Fano lineshapes in plasmon-mediated light coupling into a substrate. *Optics Express, 19*(S3), A303. doi: 10.1364/oe.19.00a303

28. Stuart, H. R., & Hall, D. G. (1998). Island size effects in nanoparticle-enhanced photodetectors. *Applied Physics Letters, 73*(26), 3815–3817. doi: 10.1063/1.122903

29. Tokman, M. D., Westerhof, E., & Gavrilova, M. A. (2000). Wave power flux and ray-tracing in regions of resonant absorption. *Plasma Physics and Controlled Fusion, 42*(2), 91–98. doi: 10.1088/0741-3335/42/2/302

30. Ungureanu, C., Rayavarapu, R. G., Manohar, S., & van Leeuwen, T. G. (2009). Discrete dipole approximation simulations of gold nanorod optical properties: Choice of input parameters and comparison with experiment. *Journal of Applied Physics, 105*(10), 102032. doi: 10.1063/1.3116139

31. Willets, K. A., & Van Duyne, R. P. (2007). Localized Surface Plasmon Resonance Spectroscopy and Sensing. *Annual Review of Physical Chemistry, 58*(1), 267–297. doi: 10.1146/annurev.physchem.58.032806.104607

32. Xu, G., Tazawa, M., Jin, P., Nakao, S., & Yoshimura, K. (2003). Wavelength tuning of surface plasmon resonance using dielectric layers on silver island films. *Applied Physics Letters, 82*(22), 3811–3813. doi: 10.1063/1.1578518

33. Yee, K. S. (1966). Numerical solution of initial boundary value problems involving maxwell's equations in isotropic media. *IEEE Transactions on Antennas Propagation, 14*(3), 302–307.

34. Zayats, A. V., & Smolyaninov, I. I. (2003). Near-field photonics: surface plasmon polaritons and localized surface plasmons. *Journal of Optics A: Pure and Applied Optics, 5*(4), S16–S50. doi: 10.1088/1464-4258/5/4/353

35. Zhao, D., Ma, Z., & Zhou, W. (2010). Plasmonic field and efficiency enhancement in crystalline thin film photovoltaics. *Next Generation (Nano) Photonic and Cell Technologies for Solar Energy Conversion*. doi: 10.1117/12.861887